

# Accurate Ground-based Astrometry of Naked-eye Stars: The United States Naval Observatory Bright-Star Astrometric Database

JEFFREY A. MUNN,<sup>1</sup> JOHN P. SUBASAVAGE,<sup>2,1</sup> HUGH C. HARRIS,<sup>1</sup> AND TRUDY M. TILLEMANN<sup>1</sup>

<sup>1</sup>*U. S. Naval Observatory, Flagstaff Station, 10391 W. Naval Observatory Road, Flagstaff, AZ 86005-8521, USA*

<sup>2</sup>*The Aerospace Corporation, 2310 E. El Segundo Boulevard, El Segundo, CA 90245, USA*

## ABSTRACT

We present the United States Naval Observatory (USNO) Bright-Star Astrometric Database (UBAD), a current-epoch high-accuracy astrometric catalog. The catalog consists of 364 bright northern hemisphere stars, including all but five such stars with either  $V < 3.5$  or with  $I < 3.2$  and  $V < 6$ , as well as a large fraction of slightly fainter stars; 36 of the brightest catalog stars are not included in Gaia Early Data Release 3 (EDR3). Observations were conducted with the USNO, Flagstaff Station, Kaj Strand 61-inch Astrometric Reflector. Target stars were imaged through a small 12.5-magnitude neutral-density spot, while the remainder of the stars in the field of view were unattenuated. This allowed for unsaturated images of the bright target stars to be calibrated directly against much fainter reference stars from Gaia EDR3. The median position errors are 1.9 mas in both right ascension and declination at the catalog epoch of 2017.0, with 90% of catalog stars having errors less than 2.6 mas; systematic errors are 1 – 3 mas. Combining UBAD observations with Hipparcos-2 positions yields proper motions with median errors of 0.045 and 0.049 mas year<sup>-1</sup> in right ascension and declination, respectively, with 90% of stars having errors less than 0.1 mas year<sup>-1</sup>; systematic errors are about 0.1 mas year<sup>-1</sup>. Single-frame accuracy for positions of the target stars is typically 5 – 6 mas. Gaia EDR3 astrometry for these bright stars, which are heavily saturated in the Gaia observations, is validated over the magnitude range  $2 \lesssim G \lesssim 6$ .

## 1. INTRODUCTION

The brightest stars in the sky, including those visible to the naked eye, are used as reference sources in many government and commercial applications, including star trackers, navigation systems, and weapon systems. Before the European Space Agency’s (ESA) Gaia mission (Gaia Collaboration et al. 2016), the most accurate as-

strometry available for these bright sources was the Hipparcos-2 catalog (van Leeuwen 2007a,b), another product of ESA. For stars brighter than  $H_p = 6$ , Hipparcos-2 has typical errors for well-behaved stars of 0.1 – 0.2 mas in position and 0.1 – 0.3 mas year<sup>-1</sup> in proper motion at the catalog epoch of 1991.25. Propagating the Hipparcos-2 positions over 30 years to today, the proper motion errors lead to position errors at the current epoch of as great as 9 mas, though considerably worse for stars that do not have well-behaved solutions in Hipparcos-2, and the

errors increase linearly going forward in time. Further, the Hipparcos satellite took observations for only 3.5 years (Perryman et al. 1997) and thus was not sensitive to detecting multiple systems with periods appreciably longer than its mission lifetime.

During the building stage of the Gaia mission, the bright magnitude limit was defined to be  $G \sim 5.7$ . Given the importance of accurate bright-star astrometry, in particular for United States Department of Defense applications, the United States Naval Observatory (USNO), Flagstaff Station, commenced a program in 2012 to obtain accurate current-epoch ground-based astrometry of bright northern hemisphere stars, those that Gaia would not observe, including all such stars in the magnitude range  $3 < V < 6$ . The basic technique was to observe the bright target star through a small neutral-density spot located in front of the detector, such that only the light from the target star and its immediate vicinity is attenuated, while the rest of the field of view remains unattenuated. The first observations were conducted with a 9-magnitude neutral-density spot, allowing the target star to be directly imaged with, and thus calibrated against, reference stars more than nine magnitudes fainter. These reference stars would be unsaturated on the Gaia instrument and thus would eventually have accurate Gaia astrometry once Gaia released its first data. This technique, using the same 9-magnitude neutral-density spot in a different camera, was first developed at USNO to validate Hipparcos astrometry (Harris et al. 1997) and later to validate a program of wide-angle absolute astrometry with the Navy Precision Optical Interferometer (Stone 2004; Zavala 2011).

In 2014 the Gaia Collaboration announced that they had modified the object detection and collection algorithms on the spacecraft to allow the collection of data for the brightest stars,

though it was unclear whether they would be able to achieve the same astrometric accuracy for these stars given that their images would be heavily saturated (Martín-Fleitas et al. 2014; Sahlmann et al. 2016). In light of these developments, we decided to change the focus of our work to the very brightest stars, those that would be most challenging for Gaia. It was also realized that while Gaia was likely to provide more accurate astrometry on even these bright stars than we could achieve from the ground, our survey could provide one of the few external validations of Gaia astrometry for bright stars. The 9-magnitude neutral-density spot was replaced with a 12.5-magnitude spot and a much brighter sample of stars was targeted.

This paper presents the results of the latter survey and compares it with Gaia Early Data Release 3 (EDR3, Gaia Collaboration et al. 2021; Lindegren et al. 2021; Rowell et al. 2021; Fabricius et al. 2021). Section 2 describes the instrumentation and observations. Section 3 describes the processing of the individual observations and characterizes the quality of those observations. Section 4 describes the production of the catalog from the individual observations and compares it with Gaia and Hipparcos-2. Section 5 presents the catalog, and Section 6 summarizes our results.

## 2. OBSERVATIONS

The USNO Bright-Star Astrometric Database (UBAD) targets all northern hemisphere ( $\delta > 0^\circ$ ) stars in the original Hipparcos catalog with  $V < 3.5$ , or with  $I < 3.5$  and  $V < 6$ , with the following exceptions:

1. Polaris, at a declination  $\delta = 89^\circ 16'$ , lies above the useful declination limit of the telescope used for the survey, and thus was excluded;
2. 46 stars that were previously observed in the first survey with the 9-magnitude

neutral-density spot were excluded — all have  $V > 3.5$ , and only four have  $I < 3.2$ ;

3. an additional five stars with  $6 < V < 7$  were included, to extend the magnitude range of overlap with Gaia.

The final sample numbers 364 stars.

Observations were conducted with the USNO, Flagstaff Station, Kaj Strand 61-inch Astrometric Reflector (Strand 1964). The telescope, commissioned in 1963, was designed specifically for precise narrow-field differential astrometry and has a long history determining stellar parallaxes in both the optical (Dahn et al. 2017, and references therein) and infrared (Vrba et al. 2004). The camera was built in-house using a  $2048 \times 4102$  e2v CCD with 15-micron pixels, which in the 61-inch focal plane yields a pixel scale of  $0.2025 \text{ arcsec pixel}^{-1}$ . A clear filter covers the detector with a 5-mm diameter 12.5-magnitude neutral-density spot deposited in the center on the sky-facing surface of the filter. The target star is observed through the spot, which has measured attenuations of 12.48 magnitudes in  $V$  and 12.89 magnitudes in  $I$ .

A total of 4807 observations were obtained between March 2016 and October 2020. All observations were taken using either an SDSS  $i$  or  $z$  filter, mostly within an hour of the meridian, to minimize differential chromatic refraction (DCR). At a minimum, each star was targeted with two visits on different nights, with two observations per visit.

After the initial set of data was processed and the final catalog generated, we decided to observe a set of fainter stars to further extend the magnitude range of overlap with Gaia and thus better constrain any dependence on magnitude in Gaia’s bright-star astrometry. Thus, an additional 151 observations were obtained in  $i$  between March and May 2021, targeting stars with  $4.0 < G < 6.5$  (the survey was cut short due to a detector failure). These observations are not

used in the UBAD catalog; they are only used in Figure 9 below.

### 3. IMAGE PROCESSING

#### 3.1. Object Detection and Characterization

Figure 1 displays a typical survey image, using a non-linear scaling to reveal various features. The dark spot in the center of the frame is the area of the CCD covered by the neutral-density filter. The target bright star is visible in the center of the spot, its flux attenuated by over 12 magnitudes. Scattered light from this bright star is evident around the spot and extending at a much lower level over about half the chip. Two out-of-focus images of the target star from multiple reflections between surfaces in the camera dominate the central half of the chip. Fringing is also evident. A close-up of the portion of the image under the neutral-density spot is shown in Figure 2. The ring around the target star is present in all images, though its brightness is only a few percent of the peak brightness. The background is considerably less uniform than a typical astronomical image.

The images are flat-fielded using a median of three dome flats. As it is impossible to get adequate counts under the neutral-density spot without saturating the rest of the CCD, an archival flat produced before the spot was installed is used for the region under the spot; there is no way to track changing dust spots in that portion of the image. SExtractor (Bertin & Arnouts 1996) is used to detect and measure stars on the images. A smaller bin size for the sky is used than usual, to better track the varying background. SExtractor is run separately on the portion of the image under the neutral-density spot, with tweaked deblending parameters so as not to deblend the ring from the target star. Centers are measured using SExtractor’s windowed first-order moments (XWIN\_IMAGE and YWIN\_IMAGE).

#### 3.2. Astrometric Calibration

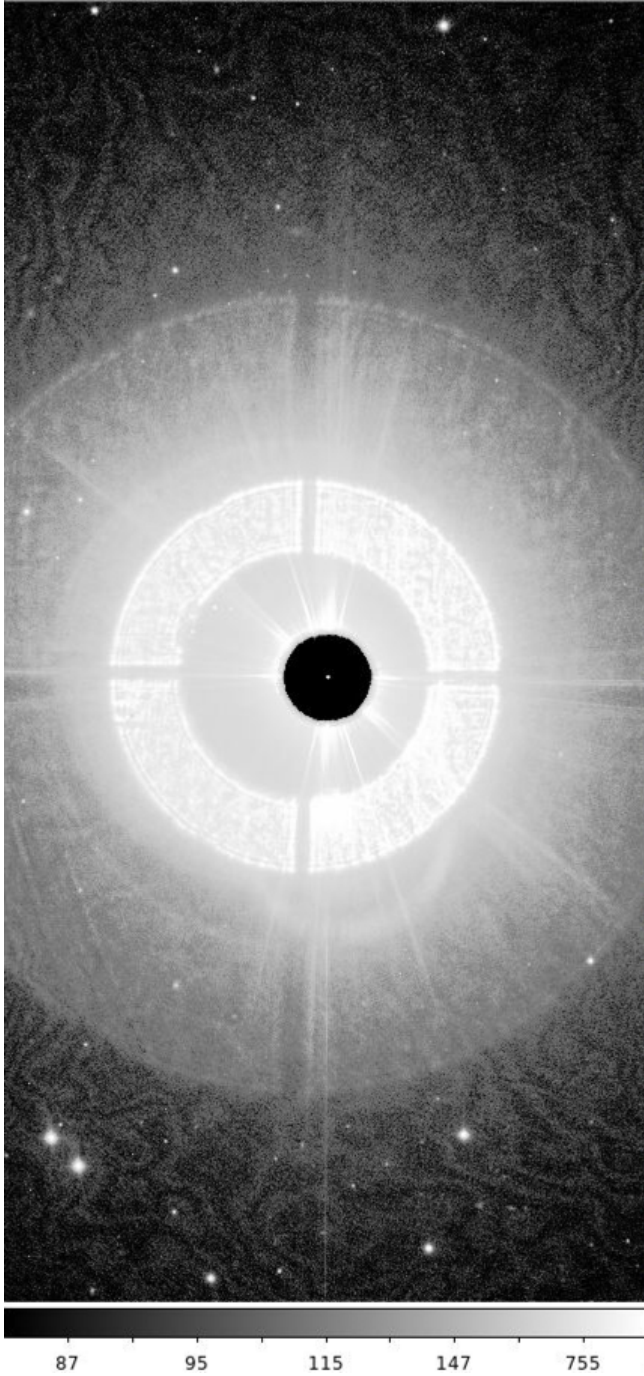


**Figure 1.** Typical survey image, taken through the *i* filter. The color bar indicates the non-linear scaling used to highlight various features in the image.

Each survey image was astrometrically calibrated against reference stars from Gaia EDR3 using custom software, built using several invaluable community software packages high-

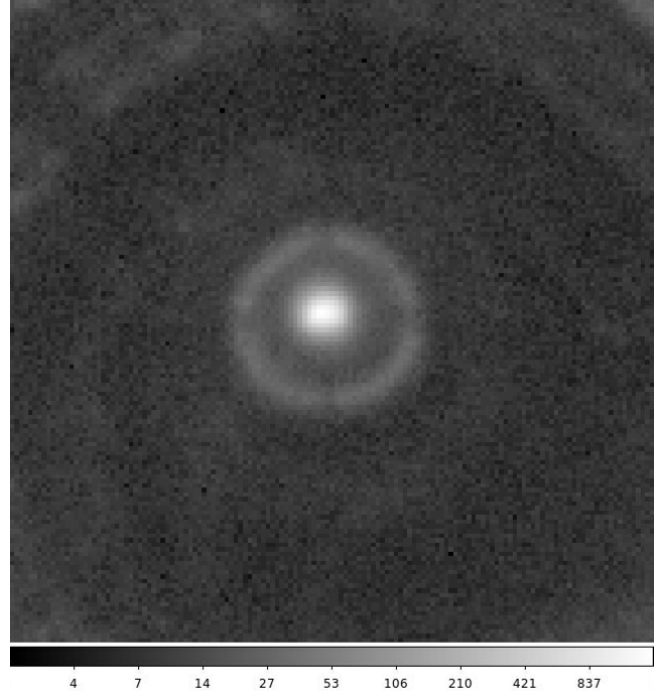


**Figure 2.** Close-up under the neutral-density spot of the image displayed in Figure 1, using a log scaling to highlight low-level features in the image.

lighted below. The following cuts were applied to the Gaia catalog to yield reliable astrometric calibrators:

1. `astrometric_params_solved` = 31 or 95 (5- or 6-parameter solution),
2. `ruwe` < 1.4,
3. `ipd_gof_harmonic_amplitude` < 0.15,
4. `ipd_frac_multi_peak` ≤ 3,
5. `ipd_frac_odd_win` < 10.

No stars were used within a large circle on the images encompassing the brightest portion of the out-of-focus images of the target star. The initial match of detected objects on the image against Gaia was performed using `astroalign` (Beroiz et al. 2020), or in those cases where `astroalign` fails, with `Astrometry.net` (Lang et al. 2010). A simple affine transformation was fit for each image; no additional optics terms were found necessary. Fits were performed after

first transforming Gaia coordinates to observed place, using place conversion routines provided by Astropy (Astropy Collaboration et al. 2013, 2018), including its interface to Essential Routines for Fundamental Astronomy (PyERFA, Kerkwijk et al. 2020), and corrected for polar motion using the Positional Astronomy Library (PALpy, Jenness & Berry 2013). Separate residual maps in  $i$  and  $z$  were created from the initial fits by calculating the clipped mean residual for the calibration stars, separately in right ascension and declination, binned in  $128 \times 128$  pixel regions of the images. The set of images used to generate the residual maps were restricted to those where 1) the rms of the residuals in both right ascension and declination were less than 12 mas, 2) the calibration used at least 30/25 stars for observations using the  $i/z$  filter, and 3) the seeing was less than 1.5/1.7 arcsec for observations using the  $i/z$  filter; looser constraints were used in  $z$  due to the smaller number of observations taken in that filter. Figures 3 and 4 display the residual maps in  $i$  and  $z$ , respectively. Residuals in  $i$  have peak-to-peak systematics of about -20 to 25 mas, while in  $z$  they are about -13 to 18 mas. The  $z$  residual map is considerably noisier as there were far fewer observations in  $z$  than  $i$ . Separate residual maps in both bands were generated spanning periods of several months, rather than over the entire survey, to look for changes in the residual maps with time; no significant changes were seen. Thus, a single residual map was used in each band for the entire survey. The pipeline was then re-run after correcting the on-chip positions, using corrections derived by interpolating the residual maps with bivariate splines.

Next, corrections for DCR were derived. For each image, a line was fit to the residuals along the parallactic angle versus the colors of the reference stars, using Pan-STARRS (Chambers et al. 2016; Magnier et al. 2020)  $r - i$  for images taken in  $i$ , and  $i - z$  for images taken in

$z$ . As this is a noisy measurement for individual frames, the ensembles for the slope and intercept values, limited to the same set of good images used to generate the residual maps, were then fit with a linear function against refraction, separately in  $i$  and  $z$ , with each fit forced to go through 0 at a refraction of 0. The results are shown in Figures 5 and 6. The fits yield the following corrections for DCR in  $i$  and  $z$  as a function of refraction and star color:

$$\text{DCR}_i \text{ (mas)} = 0.3057 \theta (r - i - 0.3893), \quad (1)$$

$$\text{DCR}_z \text{ (mas)} = 0.2541 \theta (i - z - 0.2220), \quad (2)$$

where  $\theta$  is the refraction in arcseconds.

The pipeline is then run a final time, now applying corrections for both the residual maps and DCR. Figure 7 shows the distributions of the rms residuals for the astrometric solutions for all survey images. The distributions peak near 4 mas, with 85% of the solutions having rms values less than 10 mas. Figure 8 displays the distribution of the number of calibrating stars used for each image. The sharp drop after 30 stars is because the pipeline only uses stars with better than 0.5% photometry, but will use less well-exposed stars if necessary to get at least 30 stars. Not all fields have 30 stars available, well-exposed or not.

The astrometric solutions were then used to derive ICRS astrometric-place coordinates for the target star on each image, at the epoch of the observation. DCR corrections to the target stars were applied using synthesized Pan-STARRS  $r - i$  and  $i - z$  colors from the ATLAS All-Sky Stellar Reference Catalog (Tonry et al. 2018). Note that the median parallax (as measured by Hipparcos-2) for stars in the survey is 10 mas, with nearly a third of the stars having parallaxes greater than 20 mas, easily detectable at the level of astrometry achieved by the survey.

### 3.3. Comparison with Gaia for Single Observations

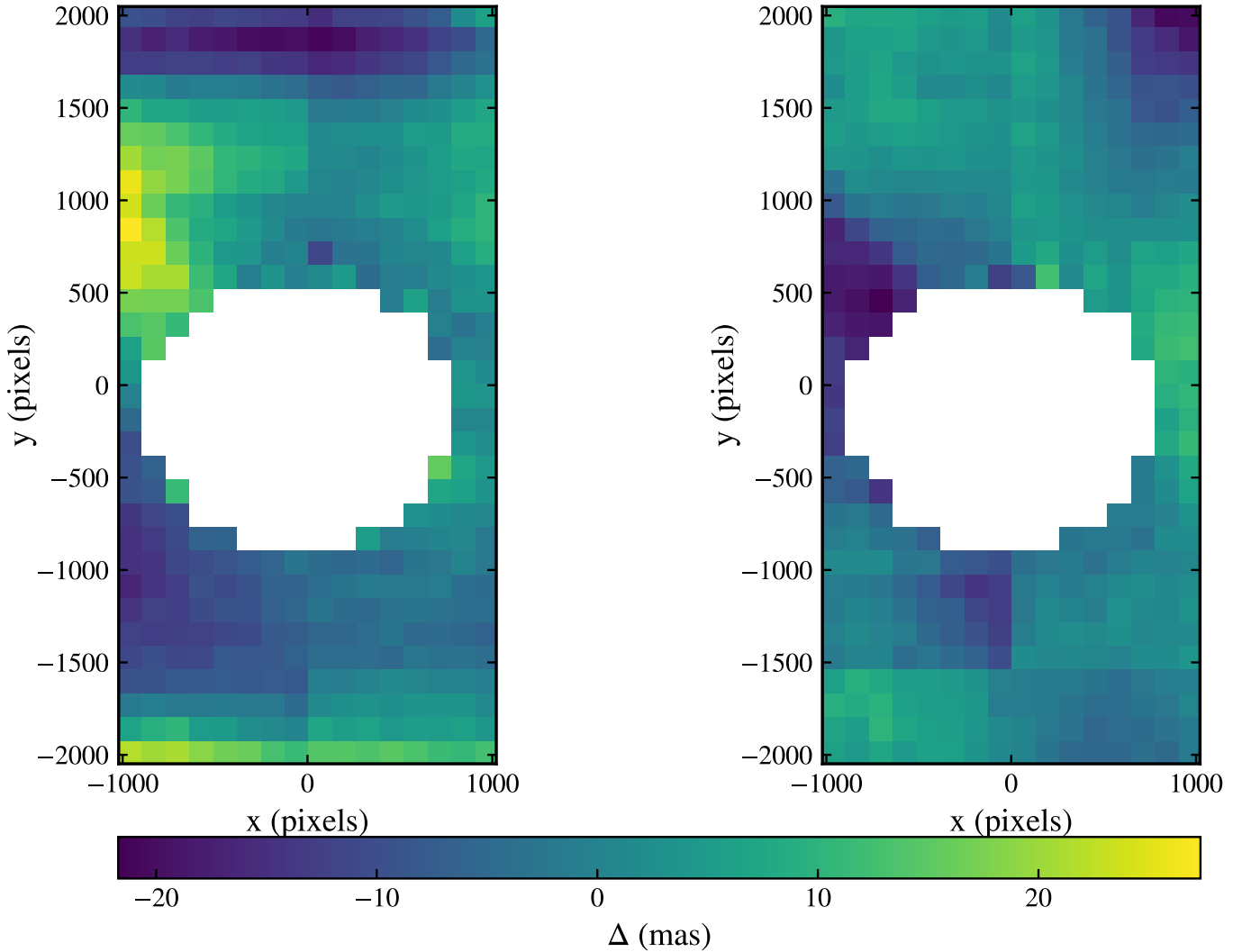


**Figure 3.** Residual maps for observations taken in  $i$  (catalog position minus observed position). The left and right panels display the maps for right ascension and declination, respectively. The CCD manufacturing process leads to discontinuities between regions on the CCD  $1024 \times 512$  pixels in size, evident in the maps. The large hole in the center of each map corresponds to the portion of the CCD not used in the astrometric calibrations due to the bright out-of-focus images of the target star.

Of the 4958 observations which comprise the UBAD survey, 4607 target a star which is in Gaia EDR3. Figures 9 and 10 plot the differences between the target star ICRS coordinates measured on each UBAD image and the matching Gaia EDR3 catalog positions, propagated to astrometric-place coordinates at the epoch of the UBAD observations using Gaia’s proper motions and parallaxes, for the 1998  $i$  and 371  $z$  observations which meet the following criteria:

1. seeing is less than 2 arcsec;

2. the astrometric calibration uses at least 15 reference Gaia stars (relaxed for a few sparse fields) and yields rms residuals of less than 20 mas in both right ascension and declination;

3. visual inspection of the target star on the UBAD image indicates no issues (blends, close neighbors, etc);

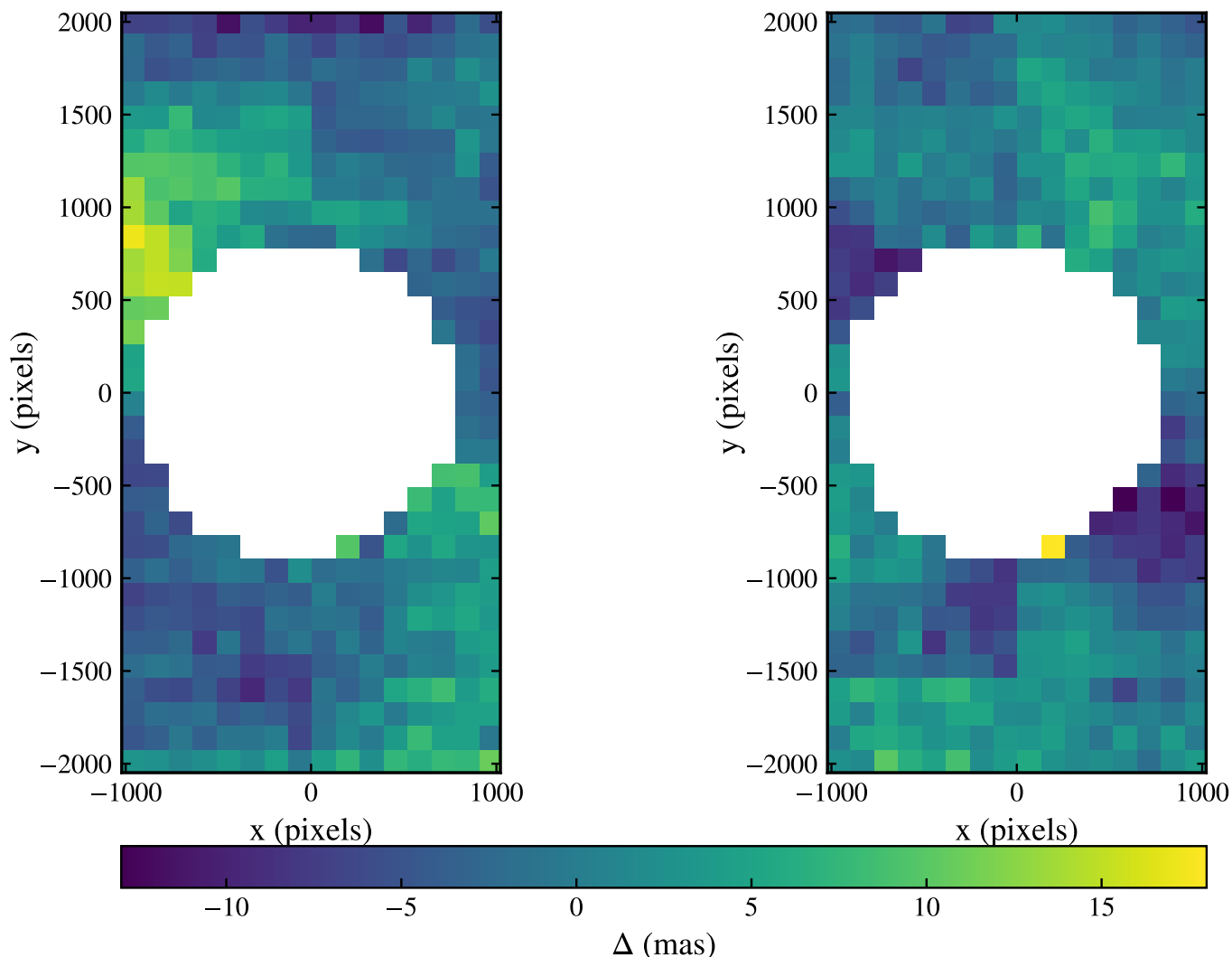


**Figure 4.** Same as Figure 3, but for observations taken in  $z$ .

4. Hipparcos-2 flags the star as a single star with a satisfactory 5-parameter astrometric fit;
5. the matching Gaia star has a 5- or 6-parameter solution and  $\text{ruwe} < 3$ .

Black and gray points are for stars in the main survey and the faint extension, respectively (no  $z$  observations were taken for the faint extension). The blue lines are the median differences for stars in the main survey. The solid and dotted orange lines indicate the medians and interquartile ranges, respectively, of the differences in bins of 100 stars in  $G$ . The comparison is excellent, with no magnitude-dependent

systematic trends in either the fully-expected median differences (discussed below) or the dispersions over the four magnitudes of overlap in  $G$  between UBAD and Gaia.

Figures 11 and 12 display histograms of the differences between the UBAD and Gaia EDR3 positions in  $i$  and  $z$  shown in Figures 9 and 10, limited to stars in the main survey. The median differences (Gaia – UBAD) in  $i$  are 8.5 and -6.6 mas in right ascension and declination, respectively. In  $z$  the median differences are 11.1 and -9.3 mas in right ascension and declination, respectively. Systematic offsets of such size are expected as the residual map was not generated under the spot, and so these off-

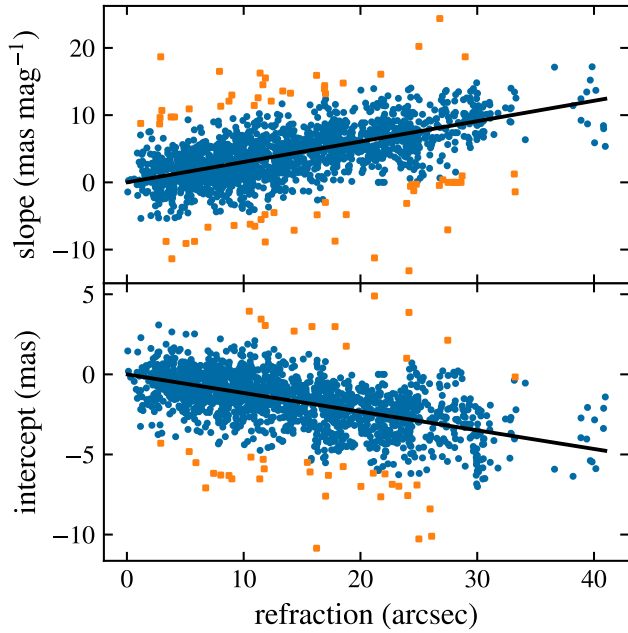


**Figure 5.** The slope and intercept values for the DCR fits for the ensemble of  $i$  images, plotted against refraction. The black lines are the fits to the ensemble, used to apply DCR corrections in  $i$ . Blue circles were included in the fits, orange squares were iteratively rejected as greater than  $3\sigma$  outliers.

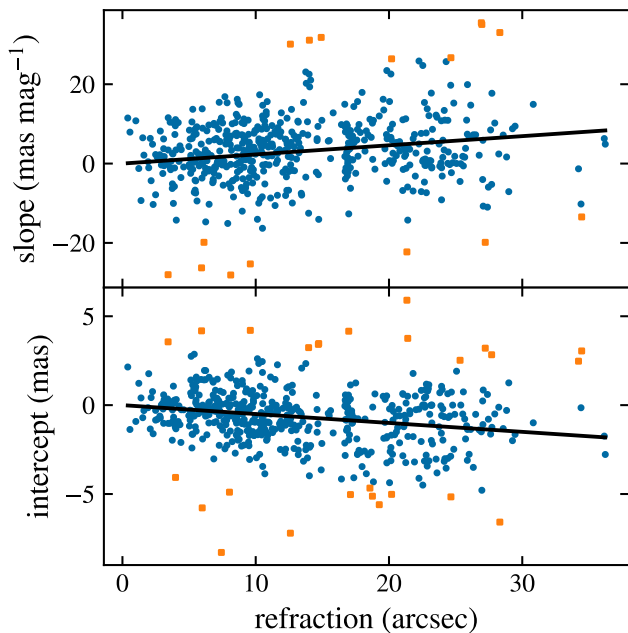


**Figure 6.** Same as Figure 5, but for the  $z$  images.

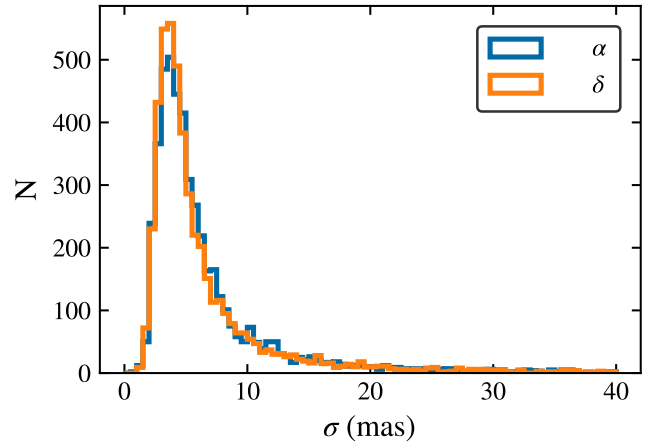


**Figure 7.** Distribution of the rms residuals for the astrometric solutions for all images in the survey, separately in right ascension and declination.

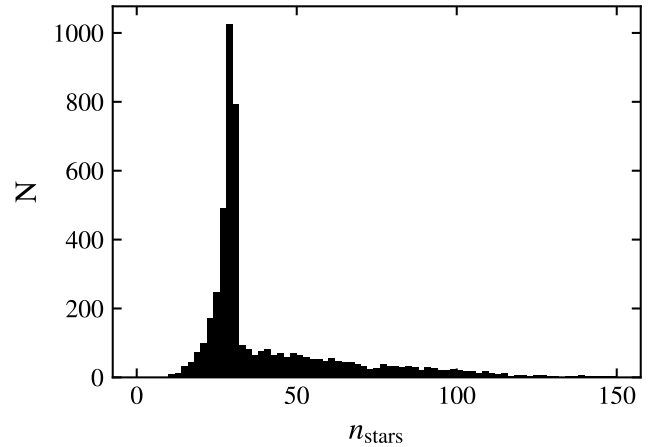


**Figure 8.** Distribution of the number of calibration stars used on each image in the survey. An additional 18 observations have more than 150 calibration stars.

sets can just be thought of as part of the residual map. These median offsets are added to all UBAD individual observation positions and are applied for all subsequent analyses. Note that since we use the offsets to calibrate UBAD, we cannot validate that Gaia EDR3 itself does not have a magnitude-independent systematic bias over the magnitude range covered by UBAD, however, given that there is no magnitude-dependent systematic offset over that magnitude range, Gaia is likely free of any such over-

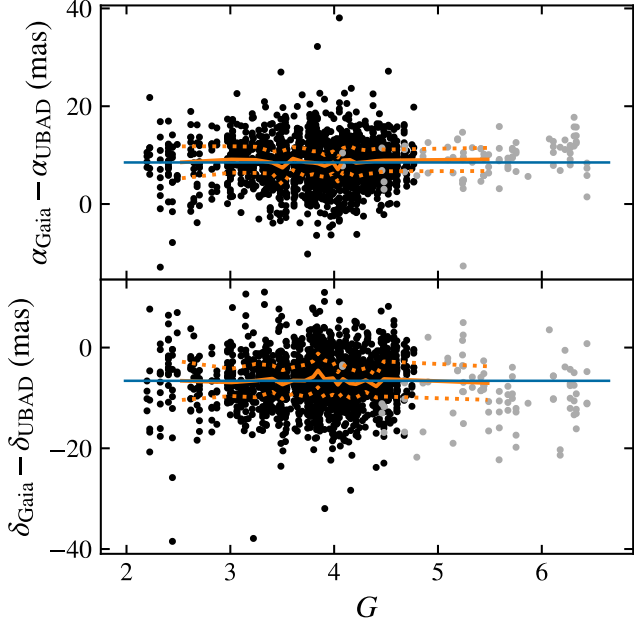


**Figure 9.** Differences between Gaia EDR3 and UBAD individual-frame positions versus Gaia  $G$  magnitude for a clean set of  $i$  observations (right ascension in the top panel, declination in the bottom panel). The black points are observations for the main survey while the gray points are for the faint survey extension, used only in this figure. The blue line is the median difference for stars in the main survey. The solid and dotted orange lines indicate the median and interquartile range, respectively, of the differences in bins of 100 stars in  $G$ .

all systematic error. The rms differences in  $i$  are 4.5 and 5.0 mas in right ascension and declination, respectively. In  $z$  the rms differences are 6.5 and 6.1 mas in right ascension and declination, respectively, giving a good indication of the single-frame astrometric accuracy of the UBAD observations (typical errors in the Gaia positions at the UBAD observation epochs are less than a mas). Different quality cuts to determine which stars are included in the analysis change the offsets by of order 0.5 mas in  $i$  and 1 – 2 mas in  $z$ , which is one indication of the size of systematic errors in the UBAD astrometry.

After correcting for the median offsets, there remain systematic differences between Gaia EDR3 and UBAD declinations as a function of

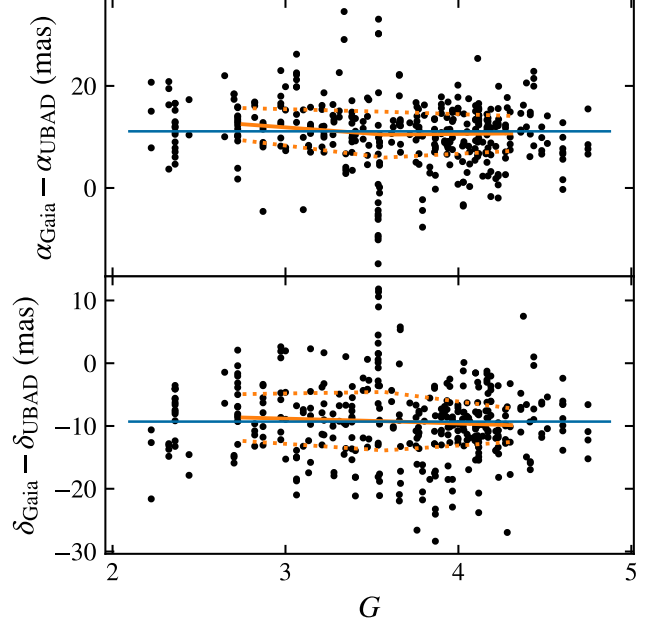


**Figure 10.** Same as Figure 9, but for  $z$  observations.

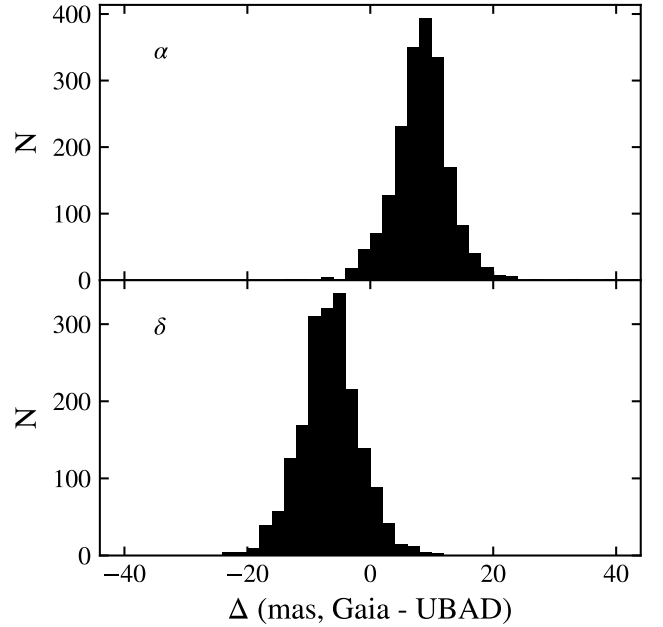


**Figure 11.** Histograms of the differences between Gaia and UBAD positions for a clean set of  $i$  observations. The differences in right ascension and declination are shown in the top and bottom panels, respectively.

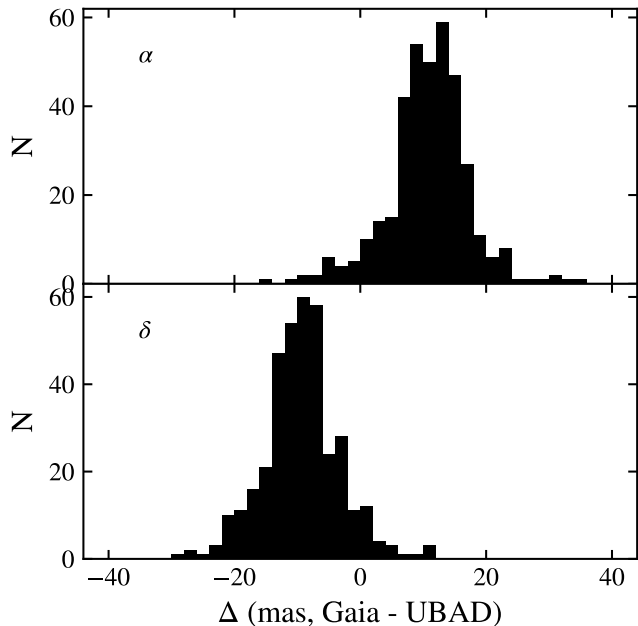


**Figure 12.** Same as Figure 11, but for  $z$  observations.

declination. Figure 13 plots these differences. The orange solid and dashed lines indicate the median and interquartile range offsets, respectively, in bins of 200 stars. No similar systematic differences are seen in right ascension. We don't understand the cause of the systematic offsets. One possible source is the ring of reflected light around the target star seen in Figure 2. The star is offset along the x-axis with respect to that ring; the x-axis is parallel to the declination axis. It's possible that as the telescope flexes at different declinations (it is on an equatorial mount), the offset between the star and the center of the ring changes, affecting the measured center of the star. The brightness of the ring is only a few percent that of the peak of the star, however, the systematic offset is small, varying roughly linearly by about 3 mas over the entire declination range. Another possible source is DCR perhaps not being fully corrected by the adopted correction model; most observations were taken within an hour of the meridian, so refraction is predominantly along declination. It is far less likely that the systematics are in the

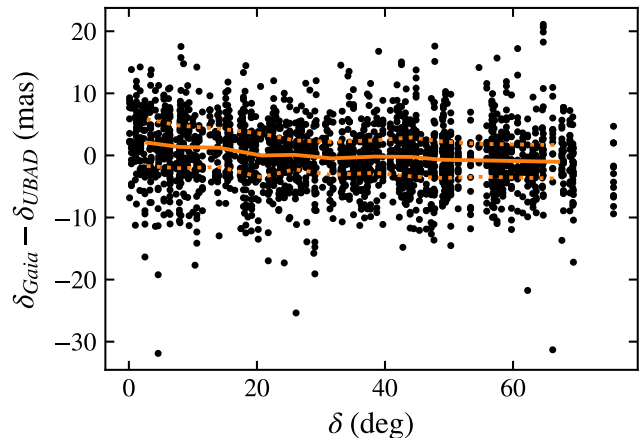


**Figure 13.** Offsets in declination between Gaia and UBAD positions as a function of declination, after correction for the median offsets. The orange solid and dashed lines are the median and interquartile range of the offsets, respectively, in bins of 200 stars.

Gaia EDR3 positions; Gaia's scanning law is roughly symmetric in ecliptic coordinates, and without concerns regarding atmospheric refraction or gravitational flexure, there is unlikely to be any systematic with declination. As the systematic is poorly understood and given that the comparison is with heavily-saturated Gaia stars, we choose not to correct it but note it as another potential source of systematic error.

### 3.4. Estimating Astrometric Errors for Single Observations

Characterizing the single-frame astrometric errors is complicated as the target star is observed in an environment (through 12.5 magnitudes of attenuation and on a background containing reflected and scattered light from the bright target star) very different from the remaining stars on the image. The errors are characterized by comparison with Gaia as the Gaia errors (less than a mas) are much smaller than the UBAD single-frame errors. Based on that comparison, it is clear that simply combining the center errors measured by SExtractor in quadrature with the calibration errors underes-

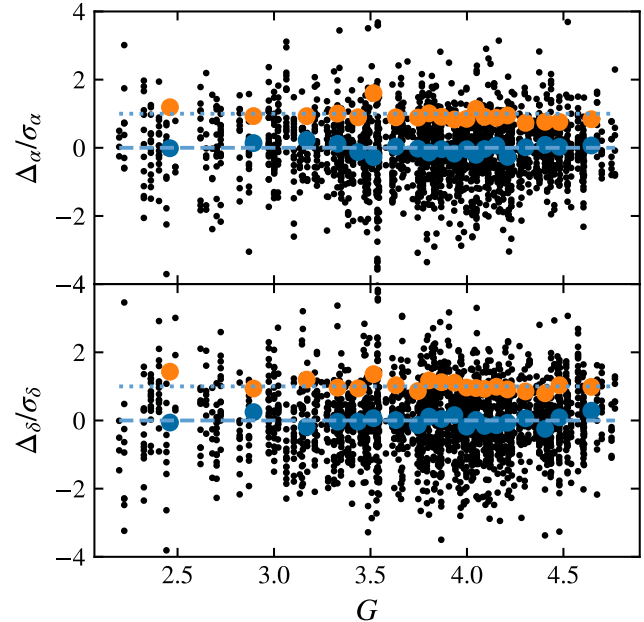
estimates the true errors. A floor of 3.5 mas is imposed on the center error of the target star on individual frames, which is then added to the center error measured by SExtractor (typically about one mas). This is then added in quadrature with the rms of the residuals of the astrometric calibration divided by the square root of the number of calibrating stars. This yields typical errors of around five mas separately in right ascension and declination, consistent with the histograms of differences between Gaia and UBAD positions seen in Figures 11 and 12.

Figure 14 plots the differences between UBAD and Gaia EDR3 positions, normalized by the expected errors in the differences based on the modified UBAD error estimates. The mean and rms differences are indicated in  $G$  magnitude bins along with the individual star differences. These normalized differences should follow a Gaussian distribution with an rms of 1 if the UBAD error estimates are valid (since the UBAD errors are significantly larger than the Gaia errors, the UBAD errors dominate this analysis); that is the case at all magnitudes.

#### 4. CATALOG ASTROMETRY

##### 4.1. Positional and Proper Motion Fits

For each survey star, position and proper motion are fit separately in right ascension and declination using the individual UBAD observations combined with the Hipparcos-2 catalog position (with some exceptions, described below). As we lack enough UBAD observations to fit a parallax, UBAD positions are corrected for parallax using the Hipparcos-2 parallax. Only UBAD observations taken in less than 2 arcsec seeing and with rms residuals in both right ascension and declination of less than 20 mas are used. All stars have at least four UBAD observations. Individual-frame positions are weighted by their inverse variance, and a linear fit is performed of position versus epoch. Since the Hipparcos-2 position errors are



**Figure 14.** Differences between Gaia and UBAD positions (Gaia – UBAD, right ascension in the top panel, declination in the bottom panel), normalized by the expected error in the differences. The black points are the individual stars. The blue and orange points are the mean and rms differences, respectively, in equal-sized bins in  $G$ . The rms values should be near one (indicated by the dotted cyan line). The dashed cyan line is a reference line at zero normalized error.

less than a mas while the UBAD errors for the restricted set of observations are all around 5 mas, this is essentially an unweighted fit to the UBAD positions with the Hipparcos-2 position as a fixed point in the fit. The fits are displayed in Figure 15.

##### **Fig. Set 15. Position and Proper Motion Fits**

Sixty two of the stars have fits in right ascension and/or declination with  $\chi^2_\nu$  values greater than 2. Thirty three of these stars were re-fit without the Hipparcos-2 position, leading to much better fits; most are known or suspected multiple systems. These include the following stars:

1. **HIP 028734, HIP 043109, HIP 054061, HIP 083895, HIP 088601, HIP 101769, HIP 104887:** Orbital binaries, fit with 7 parameters in Hipparcos-2 after taking into account the orbital parameters.
2. **HIP 014328, HIP 037279, HIP 067927, HIP 081693, HIP 095501, HIP 112158:** Orbital binaries, fit with 5 parameters in Hipparcos-2 after taking into account the orbital parameters.
3. **HIP 003092, HIP 029655, HIP 031681, HIP 086974, HIP 099874, HIP 116727:** Orbital binaries in the Sixth Catalog of Orbits of Visual Binary Stars (ORB6, [Hartkopf et al. 2001](#)), though orbital parameters were not taken into account in the Hipparcos-2 solutions.
4. **HIP 015900, HIP 028358, HIP 100587, HIP 111022:** Spectroscopic binaries in the Ninth Catalog of Spectroscopic Binary Orbits (SB9, [Pourbaix et al. 2004](#)).
5. **HIP 017358, HIP 072105:** Unresolved doubles in Hipparcos-2, fit using standard 5-parameter solutions. HIP 072105 is clearly an unresolved double in the UBAD reductions.
6. **HIP 109427:** The Hipparcos-1 fit indicates signs of accelerated motion, while the Hipparcos-2 fit is marked as stochastic. A low-mass companion was recently detected ([Steiger et al. 2021](#)).

7. **HIP 014668, HIP 058948:** Astrometric binaries in the  $\Delta\mu$  catalog of [Makarov & Kaplan \(2005\)](#).
8. **HIP 067627, HIP 079804** Unresolved photometric variable stars in Hipparcos-2.
9. **HIP 046853, HIP 102488:** These are in the Washington Double Star Catalog (WDS, [Mason et al. 2001](#)) but not marked as suspect in Hipparcos-2 or listed in the  $\Delta\mu$  catalog.
10. **HIP 101810:** No indication of possible binarity.

The remaining 29 stars with  $\chi^2_\nu$  values greater than 2 were processed including the Hipparcos-2 position, as excluding the Hipparcos-2 position did not significantly decrease the fit  $\chi^2_\nu$  values. These include:

1. **HIP 013531, HIP 023453, HIP 080816:** Orbital binaries, fit with 5 parameters in Hipparcos-2 after taking into account the orbital parameters.
2. **HIP 004427, HIP 084345, HIP 095947, HIP 097365:** Orbital binaries in ORB6, though orbital parameters were not taken into account in the Hipparcos-2 solutions.
3. **HIP 036284, HIP 104732:** Spectroscopic binaries in DB9.
4. **HIP 012706:** Unresolved double in Hipparcos-2, fit using a standard 5-parameter solution.
5. **HIP 094648:** Astrometric binary in the  $\Delta\mu$  catalog.
6. **HIP 022730, HIP 027989, HIP 091262, HIP 107259** Unresolved photometric variable stars in Hipparcos-2.
7. **HIP 050372:** Stochastic fit in Hipparcos-2.

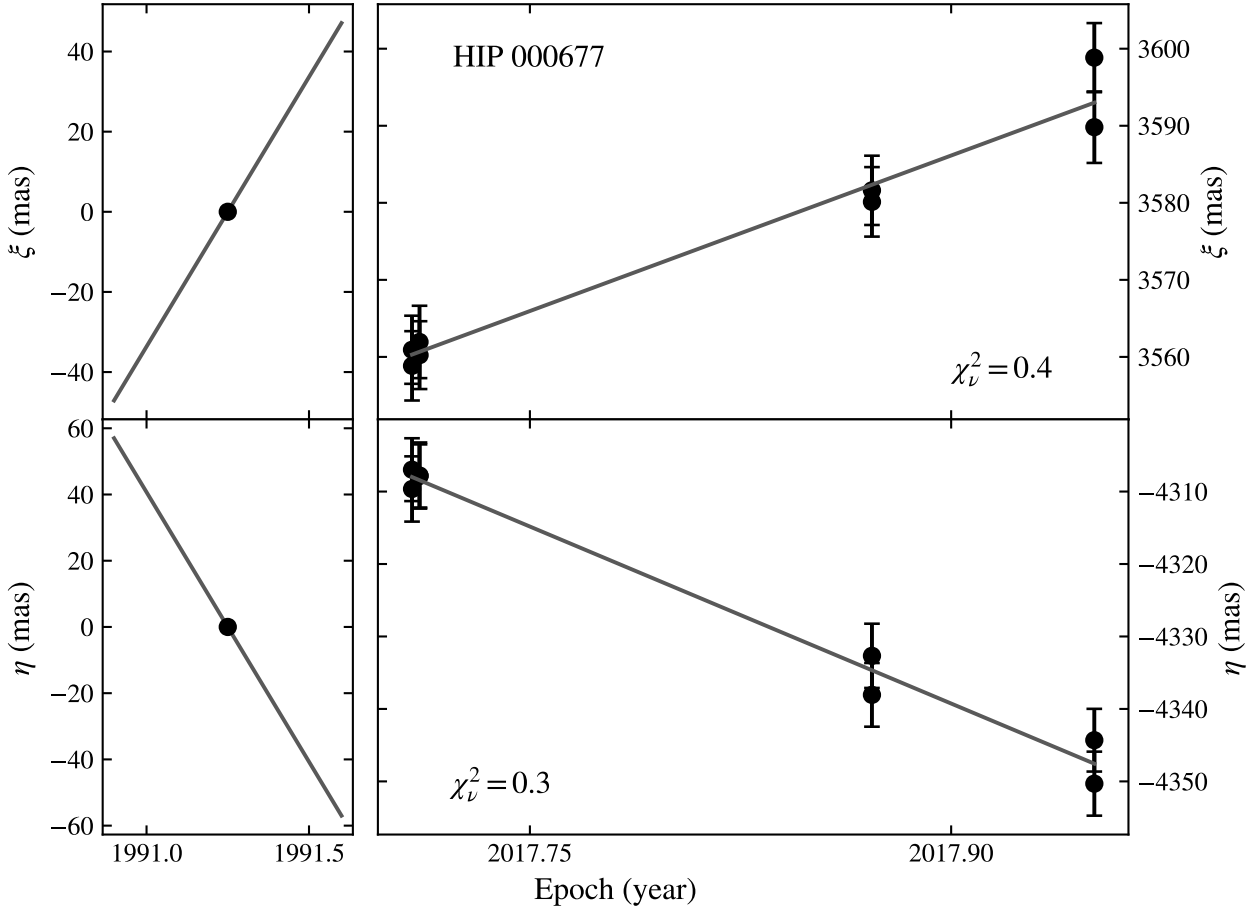


**Figure 15.** Fits to position and proper motion in the tangent plane,  $\xi$  in the top panel,  $\eta$  in the bottom panel, for HIP 000677. The circles with error bars are the individual observations and the lines are the fits. The Hipparcos-2 position (left panels) is taken as the tangent point and is plotted separate from the UBAD observations (right panels) due to the large epoch difference. The complete figure set (364 images) is available in the online journal.

8. **HIP 003179, HIP 049637, HIP 077070, HIP 084379, HIP 087833, HIP 097278, HIP 112724:** These are in the WDS but not marked as suspect in Hipparcos-2 or listed in the  $\Delta\mu$  catalog.
9. **HIP 054539, HIP 057399, HIP 083000, HIP 085693, HIP 086742, HIP 117863:** These six stars are not known or suspected doubles. Their fits have  $\chi^2_\nu$  values in right ascension/declination of 2.6/1.0, 1.0/2.5, 3.6/1.7, 0.5/3.4, 2.2/5.9, and 2.1/0.9,

respectively. The fits all look reasonable, and may just represent the tail of the  $\chi^2_\nu$  distributions.

Figure 16 displays the distribution of  $\chi^2_\nu$  values from the fits. These fits yield the astrometric parameters given in the UBAD catalog. All UBAD catalog positions are for the epoch 2017.0, roughly the median epoch of the UBAD observations.

#### 4.2. Comparison of Catalog Astrometry with Gaia and Hipparcos-2

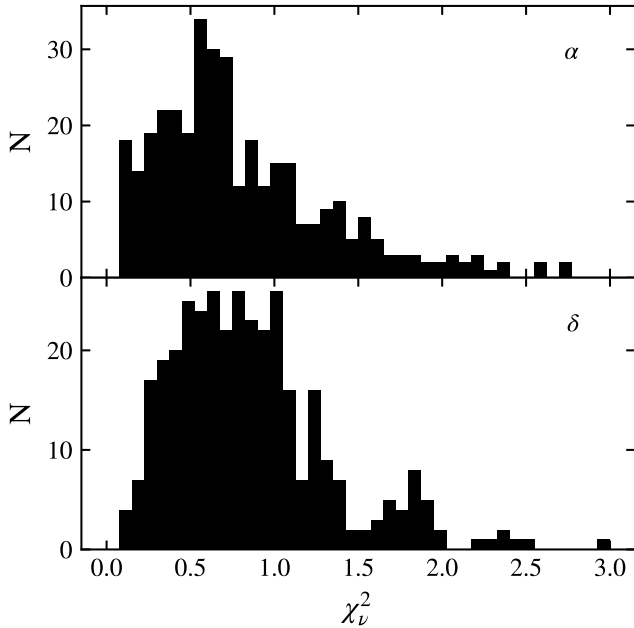


**Figure 16.**  $\chi^2_\nu$  distributions for the position and proper motion fits in right ascension (top panel) and declination (bottom panel). There are an additional 6 and 10 unplotted stars with  $\chi^2_\nu > 3$  in right ascension and declination, respectively.

Figure 17 plots the distributions of the differences between Gaia EDR3 and UBAD catalog positions, after propagating the Gaia positions to the UBAD catalog epoch. The sample is limited to stars with good fits in both UBAD ( $\chi^2_\nu < 2$  in both right ascension and declination) and Gaia (5- or 6-parameter fits and  $\mathbf{ruwe} < 3$ ), and that were fit as single stars in Hipparcos-2. The median offsets are  $-0.05$  and  $0.17$  mas in right ascension and declination, respectively, with rms scatters of  $1.8$  and  $2.3$  mas.

The median error for the Gaia positions for the stars in Figure 17, propagated to the UBAD catalog epoch, is around  $0.2$  mas, with 90% of the stars having errors less than around  $0.35$  mas. The typical errors for the UBAD stars are around  $2$  mas, consistent with the scatter in Figure 17. Thus, with position errors approximately 10 times as large as those of Gaia, UBAD can't validate Gaia bright-star astrometry to the stated accuracy in the Gaia catalog.

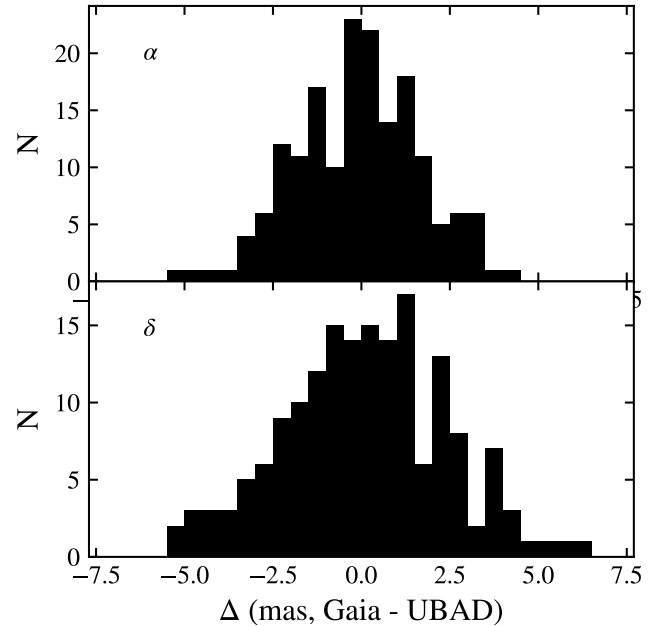


**Figure 17.** Distributions of differences in the catalog positions between Gaia and UBAD in right ascension (top panel) and declination (bottom panel).

However, UBAD does confirm Gaia's bright-star astrometry at approximately the  $2$  mas level, providing external validation of Gaia's astrometry for these heavily-saturated stars in their survey.

The formal errors in the UBAD positions appear to underestimate the true errors. Figure 18 plots the differences between the Gaia and UBAD catalog positions, normalized by the expected errors in the differences. The rms differences in equal-sized bins of the formal UBAD position error are indicated by the orange points. If the error estimates are correct, the rms values should be near one. Clearly, either the UBAD or Gaia position errors are underestimated. The Gaia errors would have to be underestimated by about a factor of eight to explain the discrepancy, which is unlikely. Thus, the final UBAD catalog position errors are corrected by adding a floor error of  $1.5$  mas in quadrature to the formal errors. Figure 19 repeats Figure 18, but now using the inflated error estimates; the rms of the position differ-

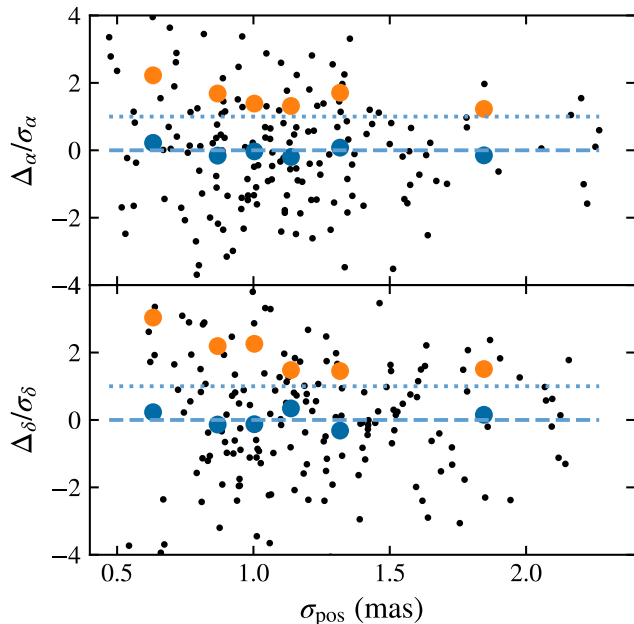


**Figure 18.** Differences between Gaia and UBAD catalog positions (Gaia – UBAD, right ascension in the top panel, declination in the bottom panel), normalized by the expected error in the differences, plotted against the formal UBAD position error. The black points are the differences for individual stars. The blue and orange points are the mean and rms differences, respectively, in equal-sized bins. If the error estimates are correct, the rms values should be near one (indicated by the dotted cyan line). The dashed cyan line is a reference line at zero normalized error.

ences now match the expected value of one for all bins in formal error.

Figures 20 and 21 display the distributions of the differences between the UBAD proper motions and those of Hipparcos-2 and Gaia EDR3, respectively, limited to the same clean sample used in Figure 17. There are no significant systematic offsets between the catalogs. The formal proper motion errors for UBAD are smaller than those for Gaia by typical factors of two to six and considerably smaller than those for Hipparcos-2, benefiting from the roughly 26-year epoch difference between Hipparcos and UBAD (clearly one could combine Gaia EDR3 and Hipparcos-2 positions to derive proper mo-

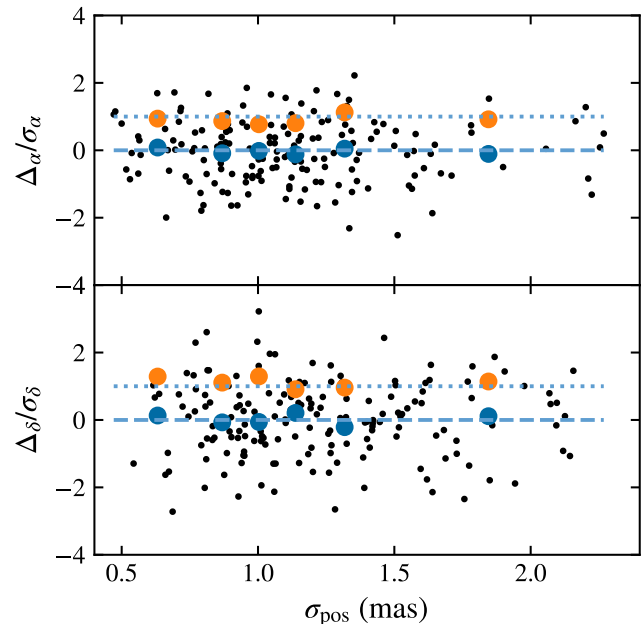


**Figure 19.** Same as Figure 18, except that the UBAD position errors used to normalize the differences now include a floor error of 1.5 mas added in quadrature with the formal error. The x-axis remains the formal error, without the addition of the floor error.

tions more accurate than UBAD’s motions). Given the underestimated UBAD position errors, it’s likely that the UBAD proper motions errors are also underestimated.

## 5. THE CATALOG

The UBAD catalog is presented in Table 1. The catalog contains 364 stars, 36 of which are not included in Gaia EDR3. All catalog positions are given for the epoch 2017.0, roughly the median epoch of the observations.

Table 2 lists the positions measured on each of the individual images comprising the survey. Positions are given as ICRS astrometric-place coordinates at the epoch of the observation (uncorrected for parallax and proper motion). Not all positions in this Table were used in compiling the final catalog (see Section 4.1).

Figures 22, 23, 24, 25, and 26 display the distributions of the catalog stars in Hipparcos-2  $H_p$  magnitude, number of UBAD observations

**Table 1.** UBAD Catalog

Hip	$\alpha$	$\sigma_\alpha \cos \delta$	$\delta$	$\sigma_\delta$	$\mu_\alpha \cos \delta$	$\sigma_{\mu_\alpha \cos \delta}$			
	(deg)	(mas)	(deg)	(mas)	(mas year <sup>-1</sup> )	(mas year <sup>-1</sup> )			
(1)	(2)	(3)	(4)	(5)	(6)	(7)			
677	2.0976353	1.78	29.0896637	1.70	134.564	0.0369			
746	2.2993446	1.74	59.1489328	1.68	523.668	0.0339			
1067	3.3089709	1.98	15.1835486	1.83	1.681	0.0499			
1168	3.6511466	1.65	20.2067096	2.45	91.341	0.0271			
2219	7.0127137	2.12	17.8932221	2.42	114.618	0.0583			

$\mu_\delta$	$\sigma_{\mu_\delta}$	$N_i$	$N_z$	Hip_used	RMS $_\alpha$	$\chi^2_{\nu,\alpha}$	RMS $_\delta$	$\chi^2_{\nu,\delta}$	Class
(mas year <sup>-1</sup> )	(mas year <sup>-1</sup> )				(mas)		(mas)		
(8)	(9)	(10)	(11)	(12)	(13)	(14)	(15)	(16)	(17)
-162.824	0.0314	8	0	1	2.60	0.378	2.18	0.282	s
-179.656	0.0293	12	0	1	2.95	0.481	2.58	0.365	s
-9.443	0.0410	11	0	1	4.14	0.756	3.77	0.571	s
1.746	0.0754	9	0	1	1.89	0.165	5.79	1.440	s
20.559	0.0740	12	0	1	5.29	1.139	6.85	1.931	s

NOTE—Column (1) is the Hipparcos identifier. Columns (2) – (5) are the ICRS catalog mean place coordinates and their errors at the catalog epoch of J2017. Columns (6) – (9) are the proper motions and their errors. Columns (10) and (11) are the number of UBAD  $i$  and  $z$  observations used in the fits, respectively. Column (12) indicates whether the Hipparcos-2 coordinate was used in the fits (1=yes, 2=no). Columns (13) – (16) are the rms of the residuals for the UBAD observations only and the reduced  $\chi^2$  of the fits. Column (17) is the visual classification of the target star on the UBAD images (s=single, n=resolved neighbor, r=resolved blend, u=unresolved blend). Table 1 is published in its entirety in the machine-readable format. A portion is shown here for guidance regarding its form and content.

used in the fits, position errors (at the catalog epoch of 2017.0), and proper motion errors for those stars which included and excluded the Hipparcos-2 position, respectively. The median position errors are 1.9 mas in both right ascension and declination; 90% of catalog stars have position errors of less than 2.6 mas in either coordinate. We estimate systematic errors in the positions of order 1 – 3 mas. For the 331 catalog stars whose fits include the Hipparcos-2 position, the median proper motion errors are 0.044 and 0.047 mas year<sup>-1</sup> in right as-

cension and declination, respectively, with 90% of such stars having proper motion errors less than 0.075 mas year<sup>-1</sup>. Those stars whose fits excluded the Hipparcos-2 position have proper motion errors of order a few mas year<sup>-1</sup>, depending on the time span of the UBAD observations for each star. Systematic errors in the proper motions are harder to estimate, as no bright-star catalog in this magnitude range has at least formally better errors in proper motions than UBAD, due to the long time span by including Hipparcos-2 positions in the proper mo-

**Table 2.** Single-epoch Positions

Epoch (year)	Hip	$\alpha$ (deg)	$\sigma_\alpha \cos \delta$ (mas)	$\delta$ (deg)	$\sigma_\delta$ (mas)
(1)	(2)	(3)	(4)	(5)	(6)
2016.190580	26727	85.1897079	6.75	-1.9425936	5.35
2016.190593	26727	85.1897094	5.69	-1.9425971	5.35
2016.190680	34912	108.3475446	4.62	51.4288135	4.62
2016.190704	34912	108.3475466	4.62	51.4288122	4.59
2016.190761	37946	116.6638232	4.83	37.5174545	4.75

T	X	$N_s$	$\text{RMS}_\alpha$	$\text{RMS}_\delta$	Seeing	Elong
(s)			(mas)	(mas)	(arcsec)	
(7)	(8)	(9)	(10)	(11)	(12)	(13)
180.0	1.279	27	23.35	9.87	1.457	1.057
360.0	1.288	27	16.50	13.13	1.604	1.035
750.0	1.042	35	3.37	3.31	1.259	1.015
600.0	1.043	35	2.52	3.00	1.177	1.039
360.0	1.002	30	3.72	3.54	1.155	1.074

NOTE—Column (1) is the observation epoch. Column (2) is the Hipparcos identifier. Columns (3) – (6) are the ICRS astrometric place coordinates and their errors at the observation epoch. Columns (7) – (8) are the observation exposure time and weighted mean airmass, respectively. Column (9) is the number of Gaia EDR3 reference stars used in the plate solution. Columns (10) – (11) are the rms residuals of the plate solution. Columns (12) and (13) are the mean FWHM and elongation of stars on the images, respectively. Table 2 is published in its entirety in the machine-readable format. A portion is shown here for guidance regarding its form and content.

tion calculations (though combining Hipparcos-2 with Gaia EDR3 would yield such a catalog). The systematic errors in the positions alone would imply systematic errors in proper motions of order  $0.1 \text{ mas year}^{-1}$ .

## 6. CONCLUSION

Gaia has revolutionized astrometry. While not designed for bright-star astrometry, Gaia EDR3 includes all but a few dozen of the brightest stars. Stars brighter than  $G \sim 5$  are saturated on the Gaia detectors, and the brightest stars are heavily saturated. Given the

importance of such stars to government and commercial interests, it is important to provide some external validation for these stars. UBAD provides such validation at the few milliarcsecond level, as well as the most accurate current-epoch astrometry for those bright northern hemisphere stars excluded from the current Gaia catalog.

UBAD gives precise positions and proper motions for 364 bright northern-hemisphere stars, including all but five such stars with either  $V < 3.5$  or with  $I < 3.2$  and  $V < 6$ ; 36 of the stars are not included in Gaia EDR3. The

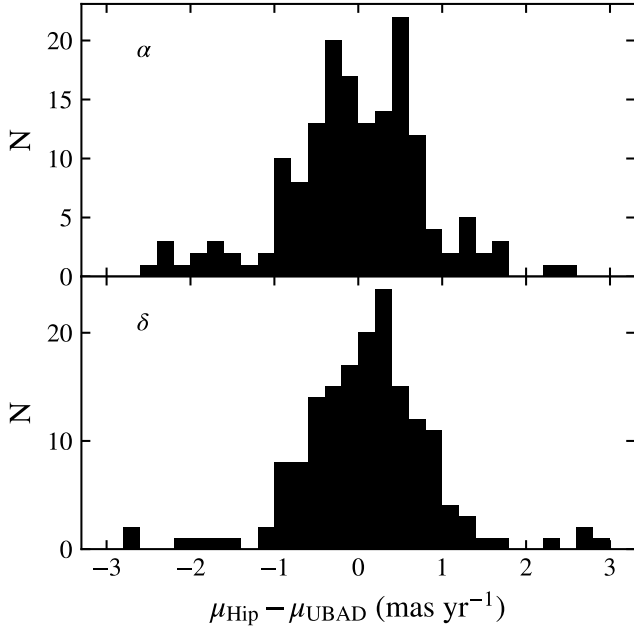


**Figure 20.** Distribution of the differences between Hipparcos-2 and UBAD proper motions for a clean sample of stars. There are an additional nine and six stars outside the histogram limits in right ascension and declination, respectively.

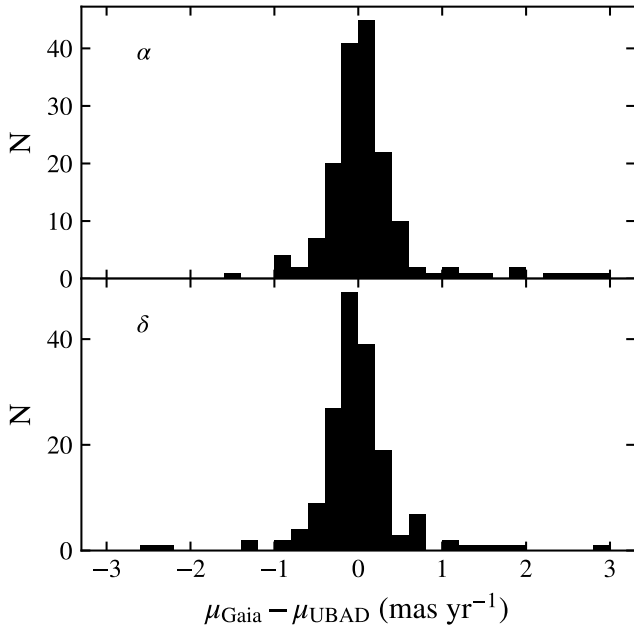


**Figure 21.** Same as Figure 20, but comparing UBAD and Gaia proper motions. There are an additional six and one stars outside the histogram limits in right ascension and declination, respectively.

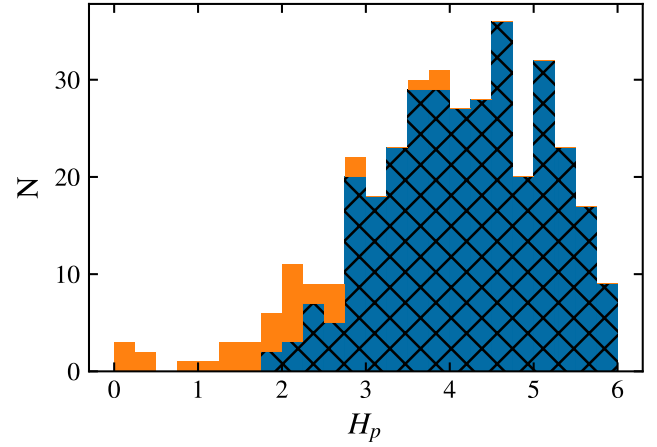


**Figure 22.** Stacked histograms of catalog stars in Hipparcos-2  $H_p$  magnitude. The hatched blue and unhatched orange histograms are for stars with and without an entry in Gaia EDR3, respectively.

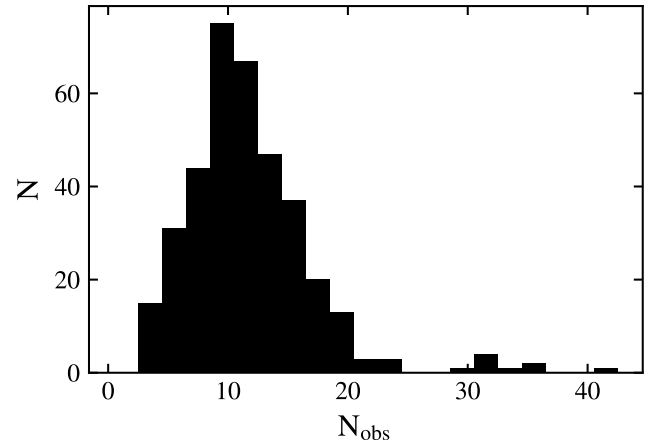


**Figure 23.** Distribution of the number of UBAD observations used in the astrometry fits.

bright target stars are exposed through a small 12.5 neutral-density spot, allowing for unsaturated images of the target stars to be calibrated directly against a dense set of stars with accurate Gaia astrometry more than 12 magnitudes fainter on the same image frame. Combining multiple UBAD observations for each star with Hipparcos-2, the median position error for UBAD stars is 1.9 mas in both right ascension and declination at the catalog epoch of 2017, with 90% of the stars having errors less than 2.6 mas; systematic errors are estimated at 1 –

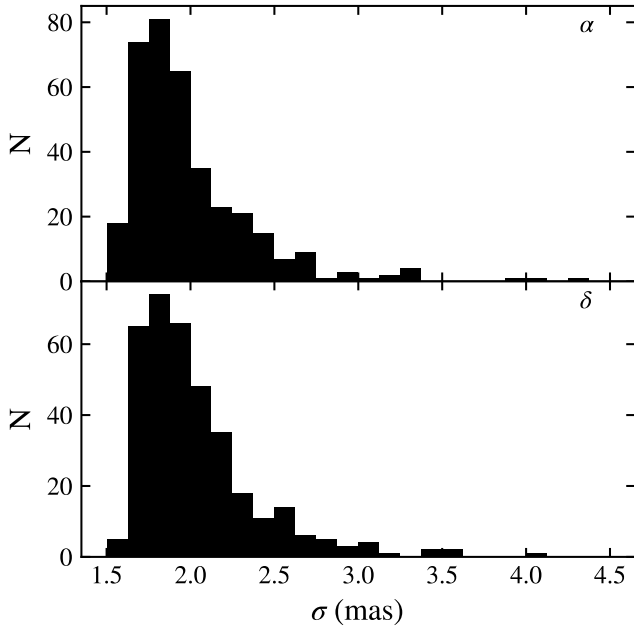


**Figure 24.** Distributions of catalog position errors (right ascension in top panel, declination in bottom panel). There are an additional two and four un-plotted stars with errors greater than 4.5 mas in right ascension and declination, respectively.

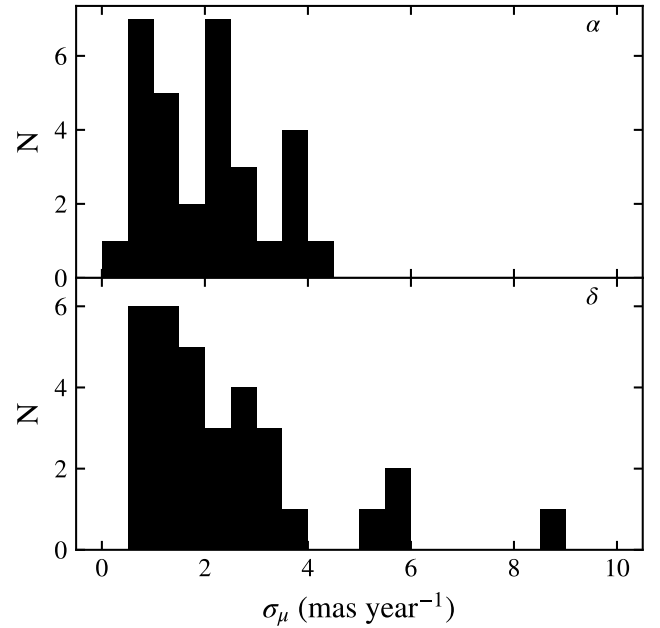


**Figure 26.** Same as Figure 25, but for the 33 stars whose fits exclude the Hipparcos-2 position. There are an additional two and one un-plotted stars with errors greater than 10 mas year<sup>-1</sup> in right ascension and declination, respectively.

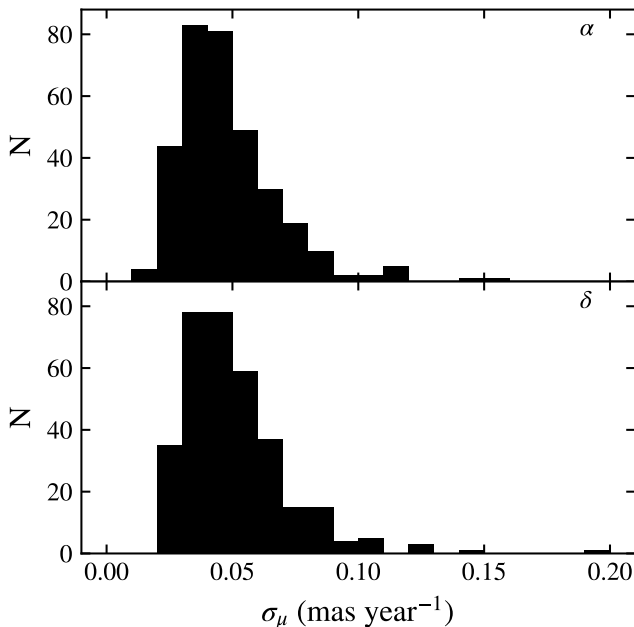


**Figure 25.** Distributions of catalog proper motion errors for the 331 stars whose fits include the Hipparcos-2 position (right ascension in top panel, declination in bottom panel).

3 mas. For those stars that include Hipparcos-2 in their solution, the median error in proper motion is 0.045 mas year<sup>-1</sup> in right ascension and 0.049 mas year<sup>-1</sup> in declination, with 90% of stars having errors less than 0.1 mas year<sup>-1</sup>.

Coupled with a faint extension that is not included in the UBAD catalog, UBAD observations overlap Gaia in the magnitude range  $2 \lesssim G \lesssim 6$ , extending from nearly the brightest stars to the non-saturated regime for Gaia. It is not possible to calibrate any optical distortion under the neutral-density spot relative to the rest of the field of view, thus we can not constrain the possibility of an overall systematic error in Gaia in this magnitude range. However, no magnitude-dependent systematic offset between Gaia and UBAD is evident at the milliarcsec level; as the comparison extends into the non-saturated regime for Gaia, an overall systematic error in Gaia is unlikely. After correction for the median offset between UBAD and

Gaia, UBAD positions are consistent with Gaia to approximately 2 mas, providing external validation of Gaia’s bright-star astrometry to that level.

Gaia fundamentally changes the nature of ground-based astrometry. By providing a dense set of calibrating stars with sub-milliarcsecond positions, it changes the field from one dominated by errors in reference catalogs to one dominated by instrumentation and atmospheric limitations. There remains a role for ground-based astrometry with small telescopes in the Gaia era. A telescope such as the 61-inch, which has been producing sub-milliarcsecond differential astrometry for decades, can now produce milliarcsecond or better absolute astrometry, with the potential for significant impacts in the study of solar system bodies, resident space objects, and similar fields with astrometric requirements beyond what Gaia provides.

We gratefully acknowledge the work of the outstanding engineering group at USNO, Flagstaff Station (some now retired), including Mike Divittorio, Fred Harris, Mike Schultheis, Al Rhodes, and Andrew Cenko. We also thank Bob Zavala for helpful comments on the text.

This work has made use of data from the European Space Agency (ESA) mission *Gaia* (<https://www.cosmos.esa.int/gaia>), processed by the *Gaia* Data Processing and Analysis Consortium (DPAC, <https://www.cosmos.esa.int/web/gaia/dpac/consortium>). Funding for the DPAC has been provided by national institutions, in particular the institutions participating in the *Gaia* Multilateral Agreement.

The Pan-STARRS1 Surveys (PS1) and the PS1 public science archive have been made possible through contributions by the Institute for Astronomy, the University of Hawaii, the Pan-STARRS Project Office, the Max-Planck Society and its participating institutes, the Max Planck Institute for Astronomy, Heidelberg and the Max Planck Institute for Extraterrestrial Physics, Garching, The Johns Hopkins University, Durham University, the University of Edinburgh, the Queen’s University Belfast, the Harvard-Smithsonian Center for Astrophysics, the Las Cumbres Observatory Global Telescope Network Incorporated, the National Central University of Taiwan, the Space Telescope Science Institute, the National Aeronautics and Space Administration under Grant No. NNX08AR22G issued through the Planetary Science Division of the NASA Science Mission Directorate, the National Science Foundation Grant No. AST-1238877, the University of Maryland, Eotvos Lorand University (ELTE), the Los Alamos National Laboratory, and the Gordon and Betty Moore Foundation.

This research has made use of the SIMBAD database, operated at CDS, Strasbourg, France (Wenger et al. 2000).

*Facility:* USNO:61in (ND12)

*Software:* astroalign 2.3.1 (Beroiz et al. 2020), Astrometry.net 0.80 (Lang et al. 2010), Astropy 4.2 (Astropy Collaboration et al. 2013, 2018), Astroquery 0.4.1 (Ginsburg et al. 2019),

PyERFA 1.7.1.1 (Kerkwijk et al. 2020), Matplotlib 3.3.2 (Hunter 2007), NumPy 1.19.4 (Harris et al. 2020), PALpy 1.8.1 (Jenness & Berry 2013), SciPy 1.5.3 (Virtanen et al. 2020), SExtractor 2.19.5 (Bertin & Arnouts 1996)

## REFERENCES

- Astropy Collaboration, Robitaille, T. P., Tollerud, E. J., et al. 2013, *A&A*, 558, A33, doi: [10.1051/0004-6361/201322068](https://doi.org/10.1051/0004-6361/201322068)
- Astropy Collaboration, Price-Whelan, A. M., Sipőcz, B. M., et al. 2018, *AJ*, 156, 123, doi: [10.3847/1538-3881/aabc4f](https://doi.org/10.3847/1538-3881/aabc4f)
- Beroiz, M., Cabral, J., & Sanchez, B. 2020, *Astronomy and Computing*, 32, 100384, doi: <https://doi.org/10.1016/j.ascom.2020.100384>
- Bertin, E., & Arnouts, S. 1996, *A&AS*, 117, 393, doi: [10.1051/aas:1996164](https://doi.org/10.1051/aas:1996164)
- Chambers, K. C., Magnier, E. A., Metcalfe, N., et al. 2016, arXiv e-prints, arXiv:1612.05560. <https://arxiv.org/abs/1612.05560>
- Dahn, C. C., Harris, H. C., Subasavage, J. P., et al. 2017, *AJ*, 154, 147, doi: [10.3847/1538-3881/aa880b](https://doi.org/10.3847/1538-3881/aa880b)
- Fabrizius, C., Luri, X., Arenou, F., et al. 2021, *A&A*, 649, A5, doi: [10.1051/0004-6361/202039834](https://doi.org/10.1051/0004-6361/202039834)
- Gaia Collaboration, Prusti, T., de Bruijne, J. H. J., et al. 2016, *A&A*, 595, A1, doi: [10.1051/0004-6361/201629272](https://doi.org/10.1051/0004-6361/201629272)
- Gaia Collaboration, Brown, A. G. A., Vallenari, A., et al. 2021, *A&A*, 649, A1, doi: [10.1051/0004-6361/202039657](https://doi.org/10.1051/0004-6361/202039657)
- Ginsburg, A., Sipőcz, B. M., Brasseur, C. E., et al. 2019, *AJ*, 157, 98, doi: [10.3847/1538-3881/aafc33](https://doi.org/10.3847/1538-3881/aafc33)
- Harris, C. R., Millman, K. J., van der Walt, S. J., et al. 2020, *Nature*, 585, 357, doi: [10.1038/s41586-020-2649-2](https://doi.org/10.1038/s41586-020-2649-2)
- Harris, H. C., Dahn, C. C., & Monet, D. G. 1997, in *ESA Special Publication*, Vol. 402, *Hipparcos - Venice '97*, ed. R. M. Bonnet, E. Høg, P. L. Bernacca, L. Emiliani, A. Blaauw, C. Turon, J. Kovalevsky, L. Lindegren, H. Hassan, M. Bouffard, B. Strim, D. Heger, M. A. C. Perryman, & L. Woltjer, 105–108
- Hartkopf, W. I., Mason, B. D., & Worley, C. E. 2001, *AJ*, 122, 3472, doi: [10.1086/323921](https://doi.org/10.1086/323921)
- Hunter, J. D. 2007, *Computing in Science & Engineering*, 9, 90, doi: [10.1109/mcse.2007.55](https://doi.org/10.1109/mcse.2007.55)
- Jenness, T., & Berry, D. S. 2013, in *Astronomical Society of the Pacific Conference Series*, Vol. 475, *Astronomical Data Analysis Software and Systems XXII*, ed. D. N. Friedel, 307
- Kerkwijk, M. V., Tollerud, E., Woillez, J., et al. 2020, *liberfa/pyerfa: v1.7.1.1*, Zenodo, doi: [10.5281/ZENODO.4279480](https://doi.org/10.5281/ZENODO.4279480)
- Lang, D., Hogg, D. W., Mierle, K., Blanton, M., & Roweis, S. 2010, *AJ*, 139, 1782, doi: [10.1088/0004-6256/139/5/1782](https://doi.org/10.1088/0004-6256/139/5/1782)
- Lindegren, L., Klioner, S. A., Hernández, J., et al. 2021, *A&A*, 649, A2, doi: [10.1051/0004-6361/202039709](https://doi.org/10.1051/0004-6361/202039709)
- Magnier, E. A., Chambers, K. C., Flewelling, H. A., et al. 2020, *ApJS*, 251, 3, doi: [10.3847/1538-4365/abb829](https://doi.org/10.3847/1538-4365/abb829)
- Makarov, V. V., & Kaplan, G. H. 2005, *AJ*, 129, 2420, doi: [10.1086/429590](https://doi.org/10.1086/429590)
- Martín-Fleitas, J., Sahlmann, J., Mora, A., et al. 2014, in *Society of Photo-Optical Instrumentation Engineers (SPIE) Conference Series*, Vol. 9143, *Space Telescopes and Instrumentation 2014: Optical, Infrared, and Millimeter Wave*, ed. J. Oschmann, Jacobus M., M. Clampin, G. G. Fazio, & H. A. MacEwen, 91430Y, doi: [10.1117/12.2056325](https://doi.org/10.1117/12.2056325)
- Mason, B. D., Wycoff, G. L., Hartkopf, W. I., Douglass, G. G., & Worley, C. E. 2001, *AJ*, 122, 3466, doi: [10.1086/323920](https://doi.org/10.1086/323920)
- Perryman, M. A. C., Lindegren, L., Kovalevsky, J., et al. 1997, *A&A*, 500, 501
- Pourbaix, D., Tokovinin, A. A., Batten, A. H., et al. 2004, *A&A*, 424, 727, doi: [10.1051/0004-6361:20041213](https://doi.org/10.1051/0004-6361:20041213)
- Rowell, N., Davidson, M., Lindegren, L., et al. 2021, *A&A*, 649, A11, doi: [10.1051/0004-6361/202039448](https://doi.org/10.1051/0004-6361/202039448)

- Sahlmann, J., Martín-Fleitas, J., Mora, A., et al. 2016, in Society of Photo-Optical Instrumentation Engineers (SPIE) Conference Series, Vol. 9904, Space Telescopes and Instrumentation 2016: Optical, Infrared, and Millimeter Wave, ed. H. A. MacEwen, G. G. Fazio, M. Lystrup, N. Batalha, N. Siegler, & E. C. Tong, 99042E, doi: [10.1117/12.2231240](https://doi.org/10.1117/12.2231240)
- Steiger, S., Currie, T., Brandt, T. D., et al. 2021, *AJ*, 162, 44, doi: [10.3847/1538-3881/ac02cc](https://doi.org/10.3847/1538-3881/ac02cc)
- Stone, R. C. 2004, Positions of Bright Stars Determined With the 1.3m Telescope and ND9 Detector, U. S. Naval Observatory Internal Memo, Defense Technical Information Center Accession Number ADA511248. <https://apps.dtic.mil/sti/pdfs/ADA511248.pdf>
- Strand, K. A. 1964, *S&T*, 27, 204
- Tonry, J. L., Denneau, L., Flewelling, H., et al. 2018, *ApJ*, 867, 105, doi: [10.3847/1538-4357/aae386](https://doi.org/10.3847/1538-4357/aae386)
- van Leeuwen, F. 2007a, Hipparcos, the New Reduction of the Raw Data, Vol. 350, doi: [10.1007/978-1-4020-6342-8](https://doi.org/10.1007/978-1-4020-6342-8)
- . 2007b, *A&A*, 474, 653, doi: [10.1051/0004-6361:20078357](https://doi.org/10.1051/0004-6361:20078357)
- Virtanen, P., Gommers, R., Oliphant, T. E., et al. 2020, *Nature Methods*, 17, 261, doi: [10.1038/s41592-019-0686-2](https://doi.org/10.1038/s41592-019-0686-2)
- Vrba, F. J., Henden, A. A., Luginbuhl, C. B., et al. 2004, *AJ*, 127, 2948, doi: [10.1086/383554](https://doi.org/10.1086/383554)
- Wenger, M., Ochsenbein, F., Egret, D., et al. 2000, *A&AS*, 143, 9, doi: [10.1051/aas:2000332](https://doi.org/10.1051/aas:2000332)
- Zavala, R. T. 2011, in American Astronomical Society Meeting Abstracts, Vol. 217, American Astronomical Society Meeting Abstracts #217, 348.04